Sensors & Actuators: B. Chemical 409 (2024) 135593

Contents lists available at ScienceDirect

Sensors and Actuators: B. Chemical

journal homepage: www.elsevier.com/locate/snb

A signal amplifying photoelectrochemical immunosensor based on the synergism of Au@$CoFe_2O_4$ and CdS/$NiCo_2O_4$ for the sensitive detection of neuron-specific enolases

Na Song [a], Jingui Chen [a], Xiang Ren [a,*], Dan Wu [a], Hongmin Ma [a], Faying Li [a,b,**], Huangxian Ju [a,c], Qin Wei [a,d,**]

[a] Key Laboratory of Chemical Sensing & Analysis in Universities of Shandong, School of Chemistry and Chemical Engineering, University of Jinan, Jinan 250022, PR China
[b] School of Chemistry and Pharmaceutical Engineering, Shandong First Medical University & Shandong Academy of Medical Sciences, Taian 271016, PR China
[c] State Key Laboratory of Analytical Chemistry for Life Science, School of Chemistry and Chemical Engineering, Nanjing University, Nanjing 210023, PR China
[d] Department of Chemistry, Sungkyunkwan University, Suwon 16419, Republic of Korea

ARTICLE INFO

Keywords:
Photoelectrochemistry
CdS/$NiCo_2O_4$
Au@$CoFe_2O_4$
NSE
Bandgap-matched

ABSTRACT

Neuron-specific enolase (NSE), a marker of small cell lung cancer, is over-expressed in patient serum. To reduce the threat of lung cancer to human health and life, a rapid and effective method for the sensitive detection of NSE is necessary. In this study, a sandwich-type photoelectrochemical (PEC) immunosensor for the rapid and sensitive detection of NSE was constructed. To provide a powerful and stable photocurrent signal, the bandgap-matched CdS/$NiCo_2O_4$ was used as the substrate material. In addition, Au@$CoFe_2O_4$, which can form a step electron transfer mode with $NiCo_2O_4$, was proposed for the first time as a second antibody (Ab_2) marker to amplify photoelectric signals. The constructed signal-amplified PEC immunosensor showed good linearity in the range of 1 pg/mL – 100 ng/mL with a detection limit as low as 0.24 pg/mL (S/N=3). The constructed PEC immunosensor has shown excellent stability, selectivity, reproducibility, and repeatability. It showed recoveries in the range of 98% – 105% and relative standard deviations (RSD) within 5% in sample analysis. The method proposed in this study is expected to be more widely used in the future for the detection of other disease markers as well as environmental pollutants.

1. Introduction

In recent years, the incidence and mortality rates of lung cancer have remained high, posing a significant challenge to people's health and lives. The two types of lung cancer are non-small cell lung cancer (NSCLC) and small cell lung cancer (SCLC), of which the incidence of SCLC is higher [1]. When SCLC is diagnosed, it is usually at an advanced stage with little chance of cure [2]. In healthy individuals, neuron-specific enolase (NSE) levels are 5 – 12 ng/mL. When NSE levels exceed 35 ng/mL, there is a risk of SCLC, and when they exceed a certain concentration, there is a high likelihood of SCLC [3–5]. Therefore, it is important that the concentration of NSE in human serum can be used as one of the most important indicators for the early diagnosis of SCLC. Sensitive detection of NSE is important for early screening of lung cancer [6]. Therefore, it is urgent to find a sensitive and stable method to detect NSE concentration in human serum. Currently, a variety of approaches have been used to detect NSE, including chemiluminescence, electrochemiluminescence, and surface-enhanced Raman scattering [7–9]. In recent years, photoelectrochemistry (PEC) has received extensive attention due to its advantages of simple operation, low background signal, fast analysis speed, easy miniaturization, and high sensitivity compared with traditional detection methods [10–15]. PEC immunosensors have been widely used in the fields of early diagnosis of diseases, food safety, and environmental monitoring [16,17]. Among them, the preparation of photoelectric active materials with excellent performance is the most important for the construction of PEC immunosensors with

* Corresponding author.
** Corresponding author at: Key Laboratory of Chemical Sensing & Analysis in Universities of Shandong, School of Chemistry and Chemical Engineering, University of Jinan, Jinan 250022, PR China
E-mail addresses: chem_renx@163.com (X. Ren), lifaying89@163.com (F. Li), sdjndxwq@163.com (Q. Wei).

https://doi.org/10.1016/j.snb.2024.135593
Received 1 January 2024; Received in revised form 22 February 2024; Accepted 3 March 2024
Available online 4 March 2024

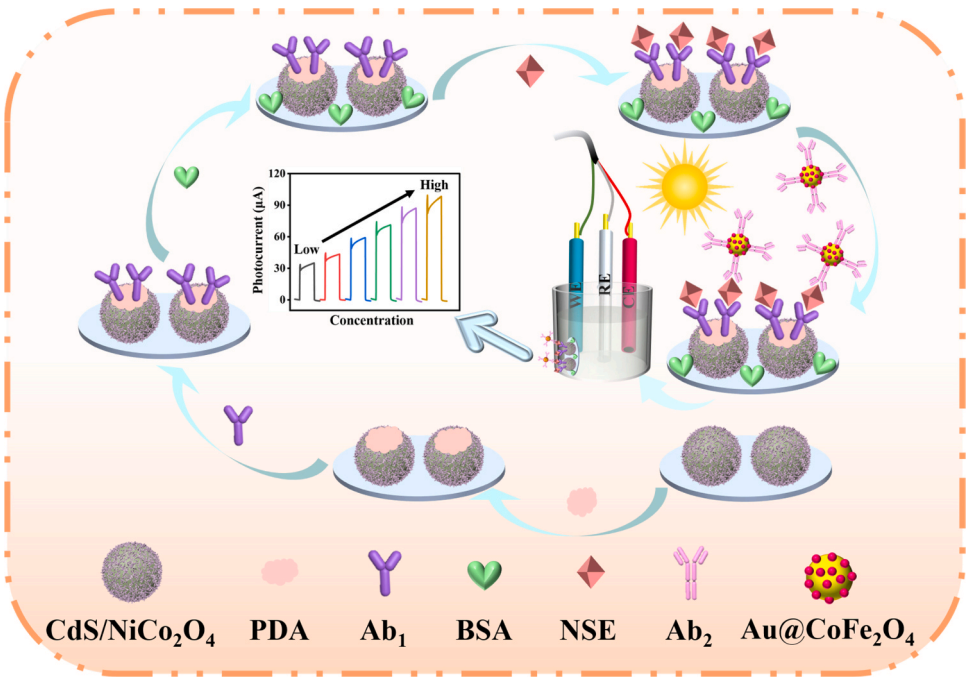

Scheme 1. Diagram of constructing PEC immunosensor.

good performance [18].

As a versatile semiconductor material, metal sulfides are very promising photoelectrically active materials with excellent physicochemical stability and suitable bandgap widths. In particular, cadmium sulfide (CdS) has attracted much attention due to its suitable band gap (2.2 − 2.4 eV), excellent photocatalytic properties, and unique structure [19,20]. However, the application of CdS is limited by its severe photocorrosion [21]. To overcome this problem, CdS can be combined with other photoactive materials to form heterostructures, which increase the photostability and suppress the rapid recombination of electron-hole (e^-/h^+) pairs [22]. Among these tested photoactive materials, $NiCo_2O_4$ with a spinel structure has attracted widespread attention due to its low cost, stable physicochemical properties, and excellent electrochemical performance. In addition, $NiCo_2O_4$ has the redox electron pairs of Ni^{3+}/Ni^{2+} and Co^{3+}/Co^{2+}, which gives it better electrical conductivity and electrochemical activity [23]. Although $NiCo_2O_4$ has been widely used in supercapacitors, electrocatalysis, and lithium-sulfur batteries, its application as a photoelectroactive substance in the PEC immunoassay has not been widely exploited [24–26]. Therefore, in this work, $NiCo_2O_4$ and CdS were composited to form heterogeneous structures, which accelerate the charge transfer and inhibit the recombination of e^-/h^+ pairs for signal enhancement.

In this study, a signal-amplifying PEC immunosensor for sensitive detection of NSE was designed. CdS/$NiCo_2O_4$ composite served as the substrate material to increase the photoelectric signal. Although the CdS/$NiCo_2O_4$ composite has a large photocurrent signal, to exhibit a strong photocurrent signal even at very low analyte concentrations. A suitable signal amplification strategy needs to be chosen to achieve the optimization of the PEC immunosensor [27]. The selection of secondary antibody (Ab_2) markers matching the bandgap of the substrate material for signal amplification of PEC immunosensors is a common approach. Cobalt ferrite ($CoFe_2O_4$) with a spinel structure has attracted attention for its excellent properties. $CoFe_2O_4$ has excellent chemical stability, optical, and electrical properties, but it has been less used in PEC immunosensor [28]. In addition, Au NPs serve as precious metals with good biocompatibility. They can be modified on the surface of $CoFe_2O_4$ to facilitate the binding of the Ab_2 to the marker and also increase the electrical conductivity. Therefore, Au@$CoFe_2O_4$ with good conductivity and photocatalytic properties was used as the Ab_2 marker for signal amplification in this work. Au@$CoFe_2O_4$ labeled PEC immunosensor with amplified signal for sensitive detection of NSE was successfully constructed. This PEC immunosensor with excellent performance provides new ideas for detecting other disease markers and environmental pollutants.

2. Experimental part

2.1. Reagents and apparatus are reported in Supplementary Material

2.1.1. Preparation of CdS, CdS/$NiCo_2O_4$, $CoFe_2O_4$ and Au@$CoFe_2O_4$

CdS, CdS/$NiCo_2O_4$, $CoFe_2O_4$, and Au@$CoFe_2O_4$ were synthesized according to the methods reported in the literature [29–31]. The synthesis process can be obtained in detail from the Supplementary Material.

2.2. Preparation of Au@$CoFe_2O_4$-Ab_2

2 mL (4 mg/mL) of Au@$CoFe_2O_4$ solution was then mixed with 1 mL (10 μg/mL) of Ab_2 solution, and incubated with shaking at 4 °C for 12 h. Finally, Au@$CoFe_2O_4$-Ab_2 was washed and dispersed with 0.1 M phosphate buffer solution (PBS, pH = 7.5).

2.3. Construction of PEC immunosensor

Scheme 1 shows the construction process of the proposed PEC immunosensors. Firstly, Indium Zinc Oxide (ITO) was washed with acetone, anhydrous ethanol, and deionized water sequentially for 30 min, and blown dry with nitrogen. Then, the bare ITO electrode was drop-coated with 30 μL of 4.10 mg/mL CdS/$NiCo_2O_4$ suspension, and the ITO/CdS/$NiCo_2O_4$ electrode was obtained by drying at room temperature. The ITO/CdS/$NiCo_2O_4$ electrodes were then incubated overnight at 4 °C in 4 mg/mL solution of dopamine (PDA) Tris-HCl (pH = 8.5), then rinsed with 0.1 M PBS (pH = 7.5) and dried. 10 μL of Ab_1 was modified on the surface of the above electrode. Then, 6 μL of bovine serum albumin (BSA, 1 *wt*%) was modified on the electrode surface and incubated at 4 °C for 2 h to block the non-specific binding sites. Next, 10 μL of NSE was modified on the surface of the above electrodes and incubated at 4 °C for 2 h. Finally, 10 μL of Au@$CoFe_2O_4$-Ab_2 was added

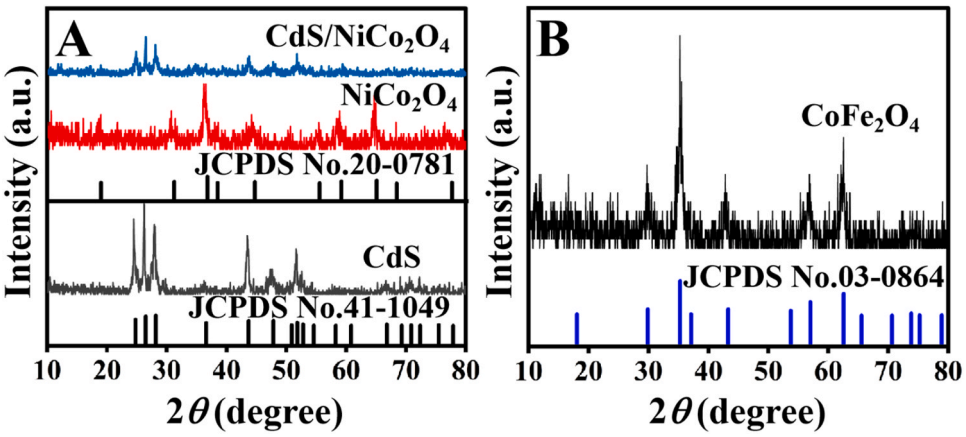

Fig. 1. (A) XRD patterns of CdS, $NiCo_2O_4$, and CdS/$NiCo_2O_4$, (B) XRD pattern of $CoFe_2O_4$.

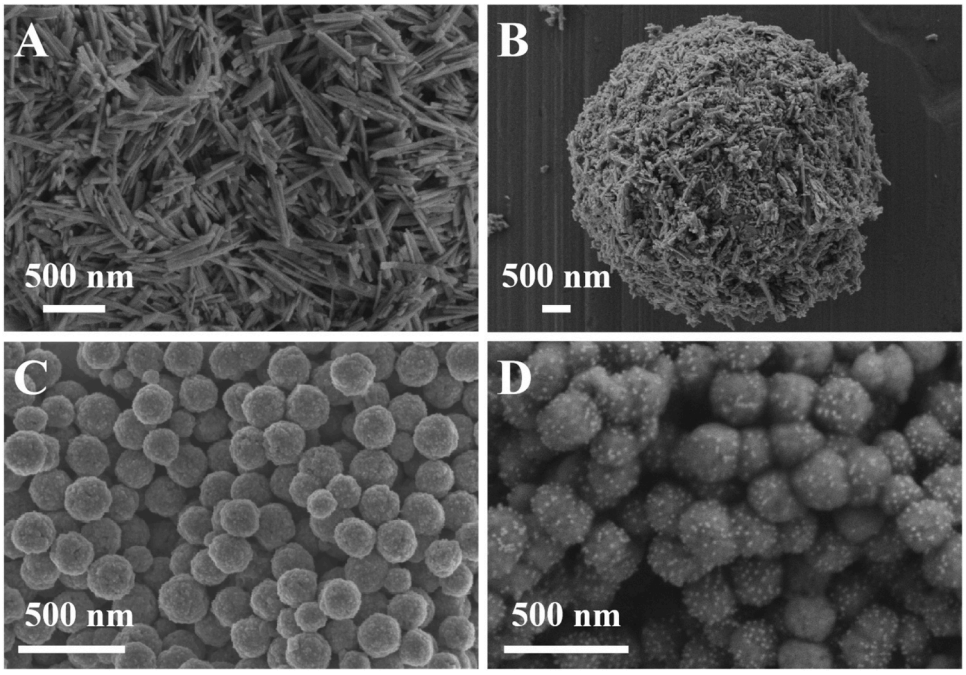

Fig. 2. (A) SEM of CdS, (B) SEM of CdS/$NiCo_2O_4$, (C) SEM of $CoFe_2O_4$, (D) SEM of Au@$CoFe_2O_4$.

dropwise to the surface of the above PEC sensing electrode and incubated for 2 h at 4 °C to form sandwich-type PEC immunosensors. After each layer of modified biomolecules, unbound material was removed with 0.1 M PBS (pH = 7.5).

3. Results and discussion

3.1. Characterization of CdS, CdS/$NiCo_2O_4$, $CoFe_2O_4$, and Au@$CoFe_2O_4$

The phase compositions and crystal structures of CdS, $NiCo_2O_4$, CdS/$NiCo_2O_4$, and $CoFe_2O_4$ were analyzed by X-ray diffraction (XRD) characterization. As shown in Fig. 1A, the synthesized CdS diffracted five strong peaks at the (100), (002), (101), (110), and (112) crystal planes, respectively. The diffraction peaks of other crystal planes are also in perfect agreement with their standard cards (JCPDS No. 41–1049), which initially indicates that the synthesis of CdS is successful. The synthesized $NiCo_2O_4$ diffracted two strong peaks at 36.70° and 64.98°, and the diffraction peaks at other positions were in perfect agreement with its standard card (JCPDS No. 20–0781). The synthesis of high-purity $NiCo_2O_4$ has been preliminarily demonstrated to be successful. The synthesized CdS/$NiCo_2O_4$ diffracted three strong peaks at 24.8°, 26.4°, and 28.0°, and there were diffraction peaks at other positions, which may be the reason for the formation of composites. The XRD pattern of $CoFe_2O_4$ in Fig. 1B shows three strong peaks at the (311), (511), and (440) crystal planes. The peaks diffracted from the other positions are also in perfect agreement with the standard card (JCPDS No. 03–0864), providing preliminary evidence for the successful synthesis of $CoFe_2O_4$.

Fig. 2A shows a scanning electron microscope (SEM) image of CdS as regular rod-like structures with size ranges around 500 nm. SEM image of $NiCo_2O_4$ is shown in Figure S1 as microscopic sphere with a dimension of around 4 μm. Fig. 2B shows an SEM image of CdS/$NiCo_2O_4$, a microsphere with a size of about 5 μm formed by depositing a layer of CdS nanorods on the surface. The elemental mapping images (Figure S2) and energy dispersive X-ray spectra (Figure S3) show that the five elements Cd, S, Ni, Co, and O are uniformly distributed in the CdS/$NiCo_2O_4$. Fig. 2C is the SEM image of $CoFe_2O_4$, which can be seen as a nanosphere with a size of around 100 nm. Fig. 2D is the SEM image of Au@$CoFe_2O_4$, and the comparison with Fig. 2C shows that Au NPs were

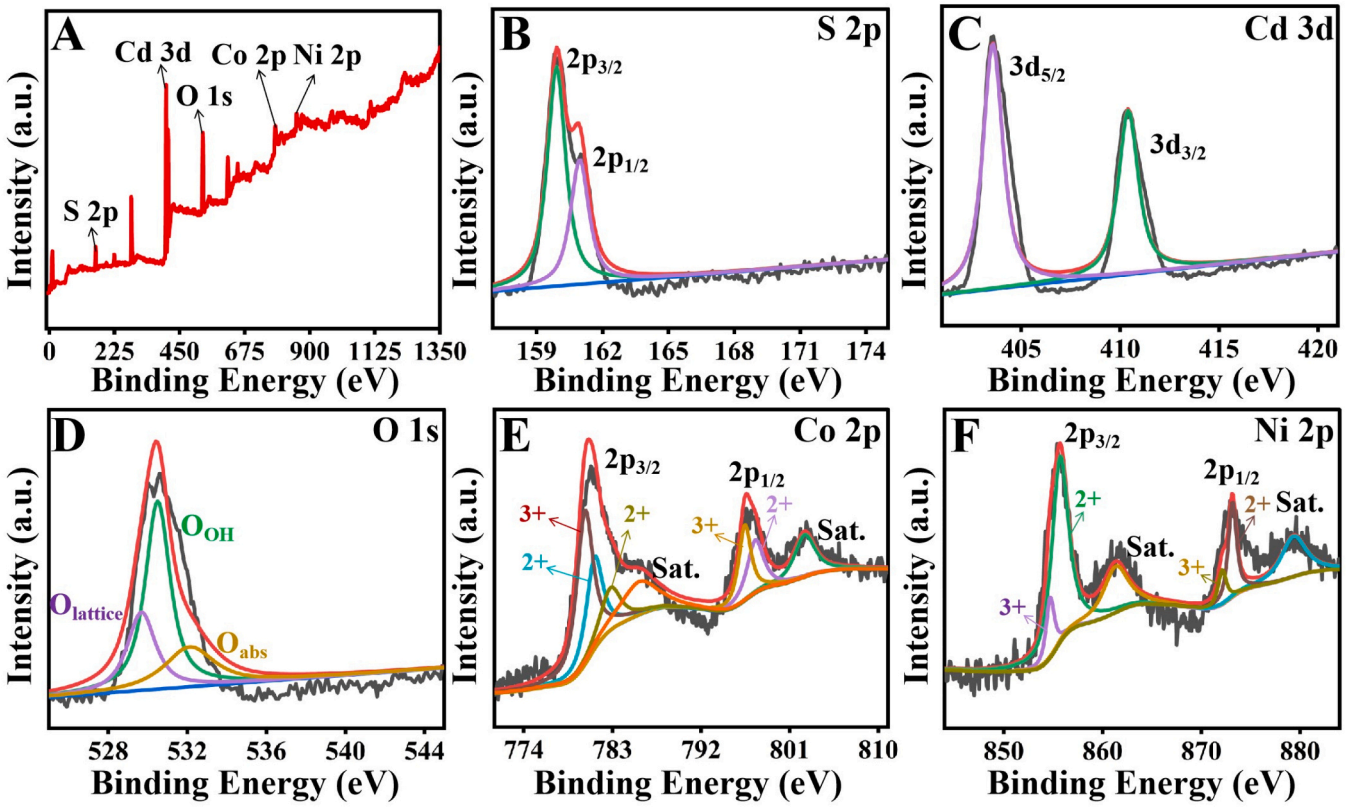

Fig. 3. (A) XPS of the $CdS/NiCo_2O_4$ composites, high-resolution XPS of (B) S 2p, (C) Cd 3d, (D) O 1 s, (E) Co 2p, and (F) Ni 2p.

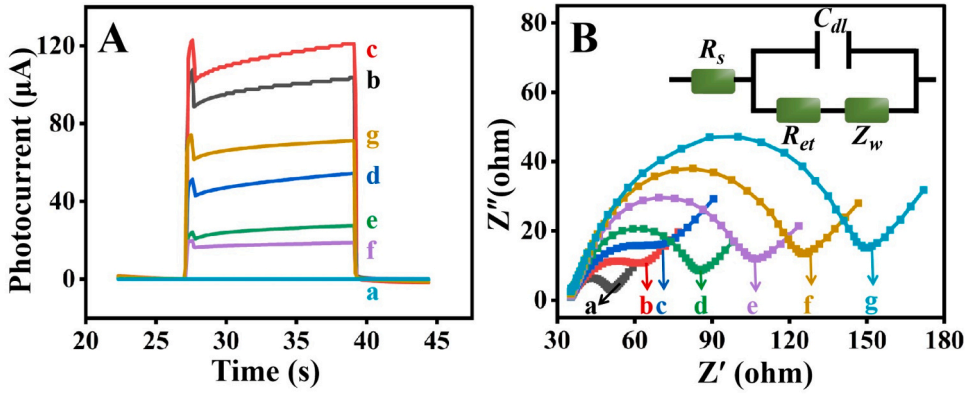

Fig. 4. (A) Photocurrent responses and (B) EIS of (a) ITO, (b) ITO/CdS/$NiCo_2O_4$, (c) ITO/CdS/$NiCo_2O_4$/PDA, (d) ITO/CdS/$NiCo_2O_4$/PDA/Ab_1, (e) ITO/CdS/$NiCo_2O_4$/PDA/Ab_1/BSA, (f) ITO/CdS/$NiCo_2O_4$/PDA/Ab_1/BSA/NSE, (g) ITO/CdS/$NiCo_2O_4$/PDA/Ab_1/BSA/NSE/Au@$CoFe_2O_4$-Ab_2 in pH 7.5 PBS containing 0.1 M AA (A) and 0.1 mol/L KCl containing 2.5 mmol/L $[Fe(CN)_6]^{4-/3-}$ (B).

successfully deposited on the surface of $CoFe_2O_4$. The results obtained from Figures S4 and S5 show that the four elements Co, Fe, O, and Au are uniformly distributed in the Au@$CoFe_2O_4$ samples. The above results tentatively demonstrate the successful synthesis of CdS, CdS/$NiCo_2O_4$, $CoFe_2O_4$, and Au@$CoFe_2O_4$.

The elemental composition and chemical valence states of the CdS/$NiCo_2O_4$ composites were further analyzed by X-ray photoelectron spectrum (XPS). The XPS pattern of CdS/$NiCo_2O_4$ demonstrated the presence of the elements S, Cd, O, Co, and Ni (Fig. 3A). In the S 2p spectra (Fig. 3B), there are two main peaks at 159.9 eV (S $2p_{3/2}$) and 160.9 eV (S $2p_{1/2}$), indicating the presence of S^{2-} of CdS in the composites. In the Cd 3d spectra (Fig. 3C), there are two main peaks at 403.5 eV (Cd $3d_{5/2}$) and 410.4 eV (Cd $3d_{3/2}$), indicating the presence of Cd^{2+} of CdS in the composites. In the O 1 s spectra (Fig. 3D), the three fitted peaks are attributed to lattice oxygen (529.7 eV), hydroxyl radicals (530.5 eV), and surface adsorbed water (532.2 eV) of $NiCo_2O_4$. In the Co 2p spectra (Fig. 3E), the two spin-orbit main peaks can be classified as at 780.2 eV (Co^{3+}(Co $2p_{3/2}$)), 781.3 eV (Co^{2+}(Co $2p_{3/2}$)), 783.0 eV (Co^{2+}(Co $2p_{3/2}$)), 796.5 eV (Co^{3+}(Co $2p_{1/2}$)) and 797.5 eV (Co^{2+}(Co $2p_{1/2}$)) of five peaks and accompanied by two satellite peaks indicating the presence of $Co^{3+}$and Co^{2+} in the composites [23]. Similarly, the Ni 2p spectra (Fig. 3F) show the presence of Ni^{2+} and Ni^{3+} in the composites. The above results further demonstrate the successful synthesis of CdS/$NiCo_2O_4$ composites.

3.2. Comparison of photocurrent signals

To demonstrate the successful construction of the immunosensor, a

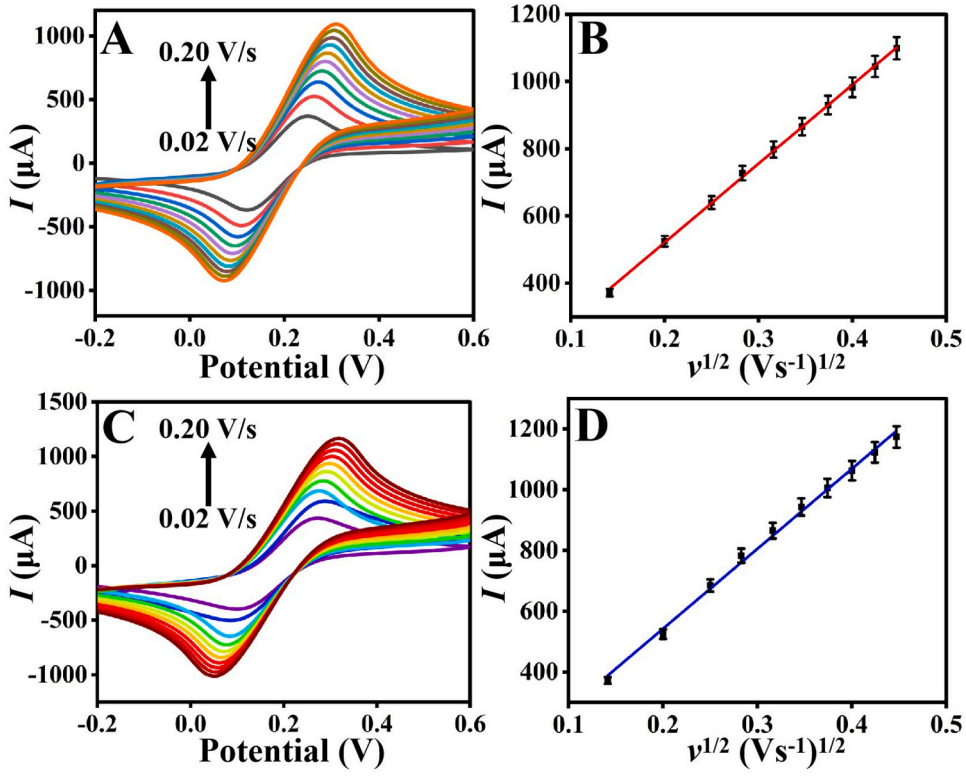

Fig. 5. (A, C) CV curves of ITO (A) and ITO/CdS/$NiCo_2O_4$ (C) in 0.1 mol/L KCl containing 5 mmol/L $[Fe(CN)_6]^{4-/3-}$ at different scanning rates, and (B, D) corresponding plots of anodic peak current to $v^{1/2}$ (error bar = SD, n = 3).

photocurrent signal comparison experiment (Fig. 4A) was conducted for the layer-by-layer modification process of the immunosensor. The photocurrent of the bare ITO is stable at around 0 μA, and its effect is negligible (curve a). After modifying only the substrate material on the ITO surface, the photocurrent was stable around 96 μA (curve b). This is because the CdS/$NiCo_2O_4$ heterostructure has good photovoltaic properties and can provide strong and stable photocurrent signals. After incubating the electrode ITO/CdS/$NiCo_2O_4$ in 4 mg/mL of PDA overnight, the electron transfer can be accelerated due to the extreme susceptibility of dopamine to oxidation, resulting in an increase of the photocurrent to 110 μA (curve c) [32]. As a non-conducting biomolecule, Ab_1 can inhibit charge transfer, resulting in an increase in the spatial potential resistance. As a result, the photocurrent (curve d) of the ITO/CdS/$NiCo_2O_4$/PDA/Ab_1 electrode decreased significantly to 48 μA. To shield the non-specific binding sites, a layer of BSA was modified on the surface of the above electrode (curve e), and the spatial potential resistance was further increased, resulting in a decrease of the photocurrent to 24 μA. When 1 ng/mL of NSE was modified on the surface of the above electrode, the photocurrent decreased to 17.3 μA (curve f). This was due to the specific recognition between Ab_1 and NSE, which further hindered the charge transfer. When Au@$CoFe_2O_4$-Ab_2 was modified on the surface of the above electrode, the photocurrent increased to 64.58 μA (curve g). This was due to the energy level matching between Au@$CoFe_2O_4$ and $NiCo_2O_4$, which can accelerate the charge transfer and achieve the amplification of the photocurrent signal. Based on the above photocurrent comparison experiments, the successful construction of the PEC immunosensor can be tentatively demonstrated. As shown in Figure S6, the photocurrent after modifying Ab_2 without labelling Au@$CoFe_2O_4$ was 12.9 μA. However, after labelling with Au@$CoFe_2O_4$, the photocurrent increased fourfold up to 64.58 μA. The above results indicate that Au@$CoFe_2O_4$ can be successfully implemented for signal amplification of the immunosensor.

3.3. Comparison of the electrochemical impedance spectroscopy

Electrochemical impedance spectroscopy (EIS) is an important tool for identifying successfully constructed PEC immunosensor [33]. Hence, AC impedance experiments were proceeded during the construction of the immunosensor to further demonstrate its successful construction (Fig. 4B). The open-circuit voltage was 0.18 V, the frequency was 0.1 ~ 1×10^5 Hz, the amplitude was 5 mV, and 0.1 M KCl and 2.5 mM $[Fe(CN)_6]^{4-/3-}$ solution were used as test solutions. The equivalent circuit of the electrolyte-electrode surface is shown in the inset of Fig. 4B, which contains the electrolyte impedance (R_s), the electrode interface resistance (R_{et}), the diffusion resistance (Z_w), and the double layer capacitance (C_{dl}). Specific data based on tests and combined with software simulations are given in Table S1. As shown in Fig. 4B, after the modification of CdS/$NiCo_2O_4$ on the ITO surface, there was a significant increase in the impedance value (27.81 Ω, curve b) compared to the bare ITO (curve a, 15 Ω). This proved that the CdS/$NiCo_2O_4$ was successfully modified on the ITO surface. When a layer of PDA was incubated on the ITO/CdS/$NiCo_2O_4$ electrode surface, the impedance increased to 35.82 Ω (curve c). When a layer of Ab_1 was modified on the surface of the above electrode, the presence of biomolecules increased the spatial site resistance, leading to a further increase in impedance to 47.55 Ω (curve d). As shown in curve e, modification of the electrode surface with a layer of BSA to shield the non-specific binding site further increased the spatial site resistance, raising the impedance to 67.83 Ω. After modification of the NSE on the electrode surface as described above (curve f), the impedance increased to 85.9 Ω. This indicated that the NSE was successfully recognized specifically by Ab_1, which further impeded the charge transfer. Eventually, the impedance value increased to 124 Ω when Au@$CoFe_2O_4$-Ab_2 is modified on the surface of the electrode, as shown in curve g. This was attributed to the presence of numerous biomolecules, resulting in an increase in spatial site resistance to a maximum. The above experimental results further demonstrate the successful construction of immunosensors.

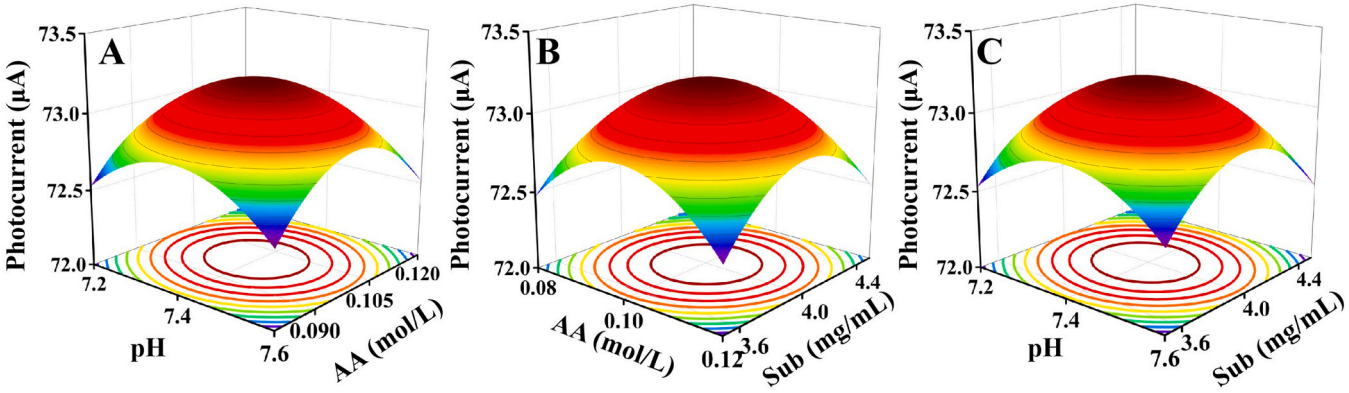

Fig. 6. (A-C) Box-Behnken experimental effect diagram of the influence of pH, AA, and CdS/$NiCo_2O_4$ concentration on photocurrent.

3.4. Electrochemical active surface area

The electroactive surface area of an electrode affects the sensitivity and active site loading of a PEC immunosensor [34]. To demonstrate whether the electroactive surface area increase after modification of CdS/$NiCo_2O_4$ on the ITO surface, cyclic voltammetry (CV) tests were carried out in 5 mM $[Fe(CN)_6]^{4-/3-}$and the results are shown in Fig. 5. All analyses for this were performed based on the Randles Sevcik equation $I = 2.69 \times 10^5 A D^{1/2} n^{3/2} v^{1/2} c$, where I is the peak value of the current related to the scanning speed, A is the electrically active surface area (cm^2), D (6.70×10^{-6} cm^2/s) is the diffusion coefficient of the $[Fe(CN)_6]^{4-/3-}$, n is the 1 number of electron transferred during the redox process, v is the scanning rate of CV (0.02 V/s − 0.20 V/s), and c is the concentration of $[Fe(CN)_6]^{4-/3-}$ (5 mM). Fig. 5A and C are, the CV curves of the bare ITO and ITO/CdS/$NiCo_2O_4$ electrodes at different scan rates, and the linear equations obtained are $I = 2346.08 \times v^{1/2} + 51.80$ ($R^2 = 0.999$) (Fig. 5B) and $I = 2633.56 \times v^{1/2} + 15.87$ ($R^2 = 0.996$) (Fig. 5D). The electrically active surface areas of the bare ITO and ITO/CdS/$NiCo_2O_4$ electrodes were obtained to be 0.67 cm^2 and 0.76 cm^2, respectively. From these results, it can be concluded that the electrically active surface area of the ITO/CdS/$NiCo_2O_4$ electrodes increased by 13.4% compared to the bare ITO.

3.5. Optimal conditions selection

To obtain the best performance of the PEC immunosensor, a traditional optimization experiment was first used to narrow down the selection [35,36]. The results obtained were a CdS/$NiCo_2O_4$ concentration of 3.5 ~ 4.5 mg/mL, pH of 7.2 ~ 7.6, and AA concentration of 0.08 ~ 0.12 mol/L. The conditions of these three experimental conditions were further optimized by the Box-Behnken experiment. The data were simulated using Design Expert software, and the true equation obtained was: $I = 376.04250 + 112.74375\,A + 166.18750B + 12.04\,C + 1.25AB + 0.025AC + 3.75BC + 67.625A^2 + 950B^2 + 1.53C^2$, where A represents the pH, B represents the AA concentration, and C represents the CdS/$NiCo_2O_4$ concentration. The optimal experimental conditions obtained are as follows, the CdS/$NiCo_2O_4$ concentration is 4.10 mg/mL, the pH is 7.5, the AA concentration is 0.1 mol/L, and the maximum photocurrent obtained is 73.1 μA (NSE concentration was 10 ng/mL). The resulting 3D images are shown in Fig. 6, where the interaction between the two factors can be explained in terms of the shape of the bottom contour. When the contour lines tend to be circular, it indicates that there is no significant mutual interaction between the two factors, and on the contrary, it means that there is a significant interaction between the two factors. From the 3D images obtained, it can be seen that the bottom contours all tend to be rounded, which means that there is no significant interaction between the two in any of the three optimized experimental conditions. In addition, the selection of AA as an electron donor to capture photogenerated holes in this study improved the photocurrent response, and the specific result is exhibited in Figure S7.

3.6. Electron transport mechanism

To further investigate how the constructed immunosensors work, possible electron transfer mechanisms were analyzed. Solid-state UV tests were perused and obtained in Figure S8A, D, and G, with bandgap

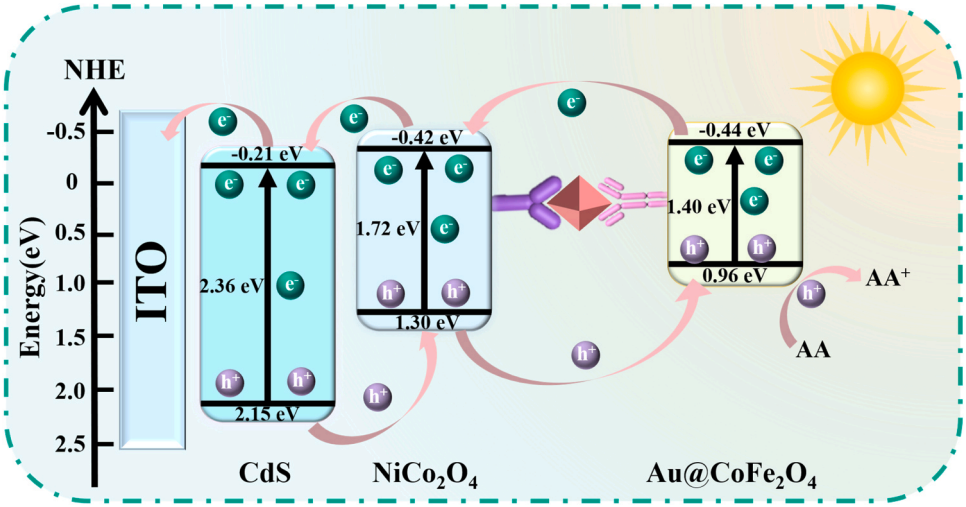

Fig. 7. Diagram of the possible mechanism of the immunosensor in 0.1 M pH 7.5 PBS containing 0.1 M AA.

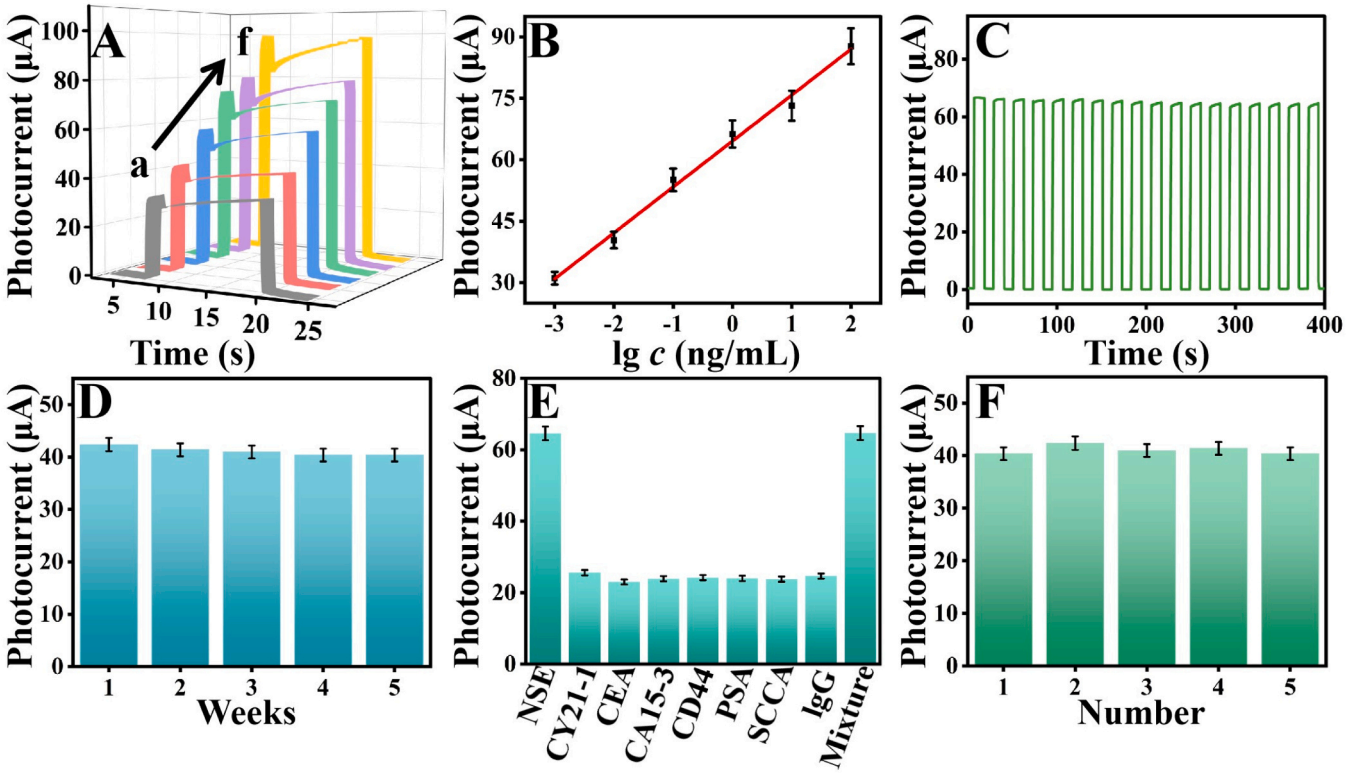

Fig. 8. (A) Photocurrent variation curves at different NSE concentrations, (a) 1 pg/mL, (b) 10 pg/mL, (c) 100 pg/mL, (d) 1 ng/mL, (e) 10 ng/mL, (f) 100 ng/mL, (B) logarithmic calibration plot of the immunosensor at different concentrations of NSE (error bar = SD, n = 5), (C) stability of immunosensor in 1 ng/mL NSE, (D) storage stability of immunosensor in 10 pg/mL NSE (error bar = SD, n = 3), (E) selectivity of the immunosensor in 1 ng/mL NSE (error bar = SD, n = 3), (F) reproducibility of immunosensor in 10 pg/mL NSE (error bar = SD, n = 3).

widths of (CdS) 2.36 eV, ($NiCo_2O_4$) 1.72 eV, and ($CoFe_2O_4$) 1.40 eV, respectively. The flat potential (E_{fb}) of CdS, $NiCo_2O_4$, and $CoFe_2O_4$ were obtained by Mott-Schottky test as −0.25 eV vs. SCE (−0.01 eV vs. NHE), −0.46 eV vs. SCE (−0.22 eV vs. NHE), and −0.48 eV vs. SCE (−0.24 eV vs. NHE), respectively. The E_{CB} of n−type semiconductors is 0 ~ 0.2 eV lower than E_{fb}. Therefore, the conduction band potential (E_{CB}) of CdS, $NiCo_2O_4$, and $CoFe_2O_4$ are −0.21 eV (vs. NHE), −0.42 eV (vs. NHE), and −0.44 eV (vs. NHE), respectively (Figure S8B, E, and H). Combining the band gap values (E_g) obtained from solid-state UV tests and the equation $E_g = E_{VB} - E_{CB}$, the valence band potentials (E_{VB}) of CdS, $NiCo_2O_4$, and $CoFe_2O_4$ were calculated to be 2.15 eV (vs. NHE), 1.30 eV (vs. NHE), and 0.96 eV (vs. NHE), respectively. Figure S8C, F, and I are UV absorption test results for CdS, $NiCo_2O_4$, and $CoFe_2O_4$ with the maximum absorption wavelengths of 534 nm, 730 nm, and 750 nm were obtained, respectively. Based on the above analysis, the possible electron transfer mechanism of the immunosensor is obtained. (Fig. 7). The electrons in $CoFe_2O_4$ are transferred from the VB to the CB and then to the CB of $NiCo_2O_4$ due to photoexcitation. Since there is a step energy relationship between CdS and $NiCo_2O_4$, the electrons are further transferred to the CB of CdS and finally to ITO. After the separation of the e^-/h^+ pairs in CdS, the hole remains in the VB and is transferred to the VB of $NiCo_2O_4$ because of an energy level difference. The hole is further transferred to the VB of $CoFe_2O_4$ and finally captured by AA.

3.7. Performance of the PEC immunosensor

The performance of the immunosensor was tested under optimal experimental conditions. The photocurrent signal increased with increasing NSE concentration (1 pg/mL − 100 ng/mL), as shown in Fig. 8A. The linear relationship between the photocurrent intensity and the logarithm of the NSE concentration is shown in Fig. 8B, with a linear equation of $I = 11.22 \lg c + 64.58$ ($R^2 = 0.991$, 95% confidence interval) and a detection limit of detection is 0.24 pg/mL (S/N=3). As shown in Table S2, the immunosensor constructed in this work for the detection of NSE has a wider detection range and a lower detection limit compared to other methods.

The stability of the immunosensor is a prerequisite for sensitive detection of NSE. Therefore, the photocurrent stability and storage stability of the immunosensor were tested. In Fig. 8C, when the light was switched on and off for 18 cycles, the photocurrent intensity was still able to maintain 96.6% of the initial photocurrent with an RSD of 1.42%. The photocurrent obtained after storing the constructed PEC immunosensor in a refrigerator at 4 °C for 1, 2, 3, and 4 weeks was 97.6%, 96.7%, 95.3%, and 95.3% of the initial photocurrent, respectively (Fig. 8D). The above results indicate that the constructed PEC immunosensor has good photocurrent stability and storage stability.

The selectivity of the PEC immunosensor is fundamental to the accuracy of the assay results. Therefore, constructed immunosensors were tested selectively using cytokeratin (CYFRA21–1), carcinoembryonic antigen (CEA), glycoconjugate antigen 15–3 (CA15–3), glycoprotein CD44, prostate-specific antigen (PSA), squamous cell carcinoma antigen (SCCA), immunoglobulin G (lgG), and a mixture of these (1 ng/mL), which may coexist with NSE. The immunosensors used for selective testing were different only for the antigens and were otherwise identical. As shown in Fig. 8E, the photocurrent values obtained after the addition of CYFRA21–1, CEA, CA15–3, CD44, PSA, SCCA, and lgG were all around 24 μA. This indicates that these four antigens were not specifically recognized. However, when the above four antigens and NSE were mixed and modified on the electrode, the detected photocurrent was the same as that of the modified pure NSE, which was about 64.58 μA. The above results indicate that the constructed immunosensor has excellent selectivity.

The reproducibility of PEC immunosensors is an important indicator for evaluating the performance of the immunosensors and is a

Table 1
Human serum samples analysis of NSE.

Samples	Added (ng/mL)	Found (ng/mL)	Recovery ($n = 5$, %)	RSD ($n = 5$, %)
1	0	5.23		1.17
	2.00	7.19	98.00	1.20
	5.00	10.18	99.00	1.74
	10.00	15.41	101.8	2.63
2	0	8.12		1.49
	2.00	10.22	105.0	1.57
	5.00	13.28	103.2	2.86
	10.00	18.53	104.1	3.30

prerequisite for repeatable experiments. Therefore, five identical PEC immunosensors were prepared in different environments to simultaneously detect NSE at a concentration of 10 pg/mL (Fig. 8F). The photocurrents obtained were 40.4 μA, 42.4 μA, 41.0 μA, 41.4 μA, and 40.4 μA with an RSD of 2.02%. The obtained test results indicate that the constructed PEC immunosensor has good reproducibility.

The repeatability of PEC immunosensors is another important indicator to evaluate the performance of the immunosensors and is a prerequisite for the reliability of the test results. Therefore, five identical PEC immunosensors were constructed to detect NSE at a concentration of 1 pg/mL, as shown in Figure S9. The test results obtained were 31.3 μA, 31.4 μA, 31.7 μA, 33.2 μA, and 32 μA with an RSD of 2.54%. The results show that the constructed PEC immunosensor has good repeatability.

3.8. Sample analysis

To validate the accuracy of the constructed immunosensor, a standard addition recovery method was used to detect the NSE content in human serum. The results of the assay are shown in Table 1, and the recoveries obtained by detecting different concentrations of NSE in human serum were in the range of 98–105%, with RSD in the range of 1.17–3.30%. This indicates that the constructed immunosensor has good precision and practical value.

4. Conclusion

In conclusion, a sandwich-type PEC immunosensor for NSE detection using $CdS/NiCo_2O_4$ as a substrate and $Au@CoFe_2O_4$ as an Ab_2 marker has been successfully constructed. By using a $CdS/NiCo_2O_4$ heterostructure with good visible light absorption as a photo-active substance, the electron transfer can be accelerated and the recombination of e^-/h^+ pairs can be inhibited, thereby increasing the photocurrent signal. In addition, the use of $CoFe_2O_4$, which matches the band gap of $NiCo_2O_4$, as an Ab_2 marker achieved the amplification of the photocurrent signal and improved the sensitivity. The proposed immunosensor demonstrated exhibited good selectivity, stability, repeatability, reproducibility, and a linear range of 1 pg/mL − 100 ng/mL with a low detection limit of 0.24 pg/mL (S/N = 3). It has good precision and practical application in the detection of human serum samples. This study provides a new idea for the detection of other disease markers.

CRediT authorship contribution statement

Xiang Ren: Methodology, Funding acquisition. **Jingui Chen:** Writing – review & editing. **Na Song:** Writing – original draft. **Qin Wei:** Methodology, Funding acquisition, Formal analysis. **Huangxian Ju:** Supervision, Formal analysis. **Faying Li:** Writing – review & editing, Formal analysis. **Hongmin Ma:** Visualization, Software. **Dan Wu:** Validation.

Declaration of Competing Interest

The authors declare that they have no known competing financial interests or personal relationships that could have appeared to influence the work reported in this paper.

Data availability

Data will be made available on request.

Acknowledgements

This study was supported by the National Natural Science Foundation of China (No. 22204059, No. 22204060, No. 22264025), the Natural Science Foundation of Shandong Province (No. ZR2021QB120, ZR2022QB021), the Foundation of Yunnan Key Laboratory of Rural Energy Engineering (Yunnan Normal University), the Special Foundation for Taishan Scholar Professorship of Shandong Province (Prof. Q. Wei), Talent Introduction and Training Program for Youth Innovation Teams in Colleges and Universities of Shandong Province, Postdoctoral Research Start-up Foundation from the University of Jinan (No. XBH2202), Shandong Medical and Health Science and Technology Project (No. 202326020474), the Young Taishan Scholars Program of Shandong Province of China (No.tsqnz20231234).

Appendix A. Supplementary Material

Supplementary data associated with this article can be found in the online version at doi:10.1016/j.snb.2024.135593.

References

[1] S. Chen, M. Li, T. Weng, D. Wang, J. Geng, Recent progress of biosensors for the detection of lung cancer markers, J. Mater. Chem. B 11 (2023) 5715–5747, https://doi.org/10.1039/d2tb02277j.
[2] J. Chen, J. Zhao, J. Feng, D. Wu, H. Ma, X. Ren, et al., Photoelectrochemical Immunosensor Based on a 1D Fe_2O_3/3D Cd-$ZnIn_{2.2}S_y$ Heterostructure as a Sensing Platform for Ultrasensitive Detection of Neuron-Specific Enolase, Anal. Chem. 94 (2022) 17396–17404, https://doi.org/10.1021/acs.analchem.2c02645.
[3] H. Li, Q. Xiao, J. Lv, Q. Lei, Y. Huang, Dopamine modified hyperbranched TiO_2 arrays based ultrasensitive photoelectrochemical immunosensor for detecting neuron specific enolase, Anal. Biochem. 531 (2017) 48–55, https://doi.org/10.1016/j.ab.2017.05.025.
[4] S.K. Arya, S. Bhansali, Lung Cancer and Its Early Detection Using Biomarker-Based Biosensors, Chem. Rev. 111 (2011) 6783–6809, https://doi.org/10.1021/cr100420s.
[5] B. Liu, Z. Xie, G. Liu, Y. Gu, S. Pan, H. Wang, Elevated neuron-specific enolase and S100 calcium-binding protein B concentrations in cerebrospinal fluid of patients with anti -N -methyl- d -aspartate receptor encephalitis, Clin. Chim. Acta 480 (2018) 79–83, https://doi.org/10.1016/j.cca.2018.01.016.
[6] N. Zhang, D. Leng, Y. Wang, Z. Ru, G. Zhao, Y. Li, et al., Split-Type Photoelectrochemical/Visual Sensing Platform Based on $SnO_2/MgIn_2S_4$/$Zn_{0.1}Cd_{0.9}S$ Composites and $Au@Fe_3O_4$ Nanoparticles for Ultrasensitive Detection of Neuron Specific Enolase, Anal. Chem. 94 (2022) 15873–15878, https://doi.org/10.1021/acs.analchem.2c03942.
[7] Y. Zheng, Y. Zhao, Y. Di, L. He, S. Liao, D. Li, et al., In vitroselection of DNA aptamers for the development of chemiluminescence aptasensor for neuron-specific enolase (NSE) detection, 15513-20, RSC Adv. 9 (2019), https://doi.org/10.1039/c9ra00785g.
[8] Y. Tang, X. Hu, Y. Liu, Y. Chen, F. Zhao, B. Zeng, An antifouling electrochemiluminescence sensor based on mesoporous $CuO_2@SiO_2$/luminol nanocomposite and co-reactant of ionic liquid functionalized boron nitride quantum dots for ultrasensitive NSE detection, Biosens. Bioelectron. 214 (2022) 114492, https://doi.org/10.1016/j.bios.2022.114492.
[9] X. Gao, P. Zheng, S. Kasani, S. Wu, F. Yang, S. Lewis, et al., Paper-Based Surface-Enhanced Raman Scattering Lateral Flow Strip for Detection of Neuron-Specific Enolase in Blood Plasma, 10104-10, Anal. Chem. 89 (2017), https://doi.org/10.1021/acs.analchem.7b03015.
[10] H. Li, J. Wang, X. Wang, H. Lin, F. Li, Perylene-Based Photoactive Material as a Double-Stranded DNA Intercalating Probe for Ultrasensitive Photoelectrochemical Biosensing, 16958-64, ACS Appl. Mater. Interfaces 11 (2019), https://doi.org/10.1021/acsami.9b04299.
[11] J.-T. Cao, J.-L. Lv, X.-J. Liao, S.-H. Ma, Y.-M. Liu, A membraneless self-powered photoelectrochemical biosensor based on $Bi_2S_3/BiPO_4$ heterojunction photoanode coupling with redox cycling signal amplification strategy, Biosens. Bioelectron. 195 (2022) 113651, https://doi.org/10.1016/j.bios.2021.113651.

[12] J.-T. Cao, J.-L. Lv, X.-J. Liao, S.-H. Ma, Y.-M. Liu, Photogenerated Hole-Induced Chemical–Chemical Redox Cycling Strategy on a Direct Z-Scheme Bi_2S_3/Bi_2MoO_6 Heterostructure Photoelectrode: Toward an Ultrasensitive Photoelectrochemical Immunoassay, Anal. Chem. 93 (2021) 9920–9926, https://doi.org/10.1021/acs.analchem.1c02175.
[13] B. Wang, L.-P. Mei, Y. Ma, Y.-T. Xu, S.-W. Ren, J.-T. Cao, et al., Photoelectrochemical-chemical-chemical redox cycling for advanced signal amplification: proof-of-concept toward ultrasensitive photoelectrochemical bioanalysis, Anal. Chem. 90 (2018) 12347–12351, https://doi.org/10.1021/acs.analchem.8b03798.
[14] Y.-X. Dong, J.-T. Cao, B. Wang, S.-H. Ma, Y.-M. Liu, Spatial-Resolved Photoelectrochemical Biosensing Array Based on a CdS@g-C_3N_4 Heterojunction: A Universal Immunosensing Platform for Accurate Detection, ACS Appl. Mater. Interfaces 10 (2018) 3723–3731, https://doi.org/10.1021/acsami.7b13557.
[15] X. Li, F. Ma, M. Yang, J. Zhang, Nanomaterial based analytical methods for breast cancer biomarker detection, Mater. Today Adv. 14 (2022) 100219, https://doi.org/10.1016/j.mtadv.2022.100219.
[16] J. Chen, J. Zhao, R. Feng, H. Ma, H. Wang, X. Ren, et al., Competitive photoelectrochemical aptamer sensor based on a Z-scheme Fe_2O_3/g-C_3N_4 heterojunction for sensitive detection of lead ions, J. Hazard. Mater. 459 (2023) 132122, https://doi.org/10.1016/j.jhazmat.2023.132122.
[17] J. Chen, N. Song, N. Zhang, Z. Gao, D. Wu, H. M, et al., Smartphone-controlled portable photoelectrochemical immunosensor for point-of-care testing of carcinoembryonic antigen, Chem. Eng. J. 473 (2023) 145276, https://doi.org/10.1016/j.cej.2023.145276.
[18] J. Zhang, X. Xue, Y. Du, J. Zhao, H. Ma, X. Ren, et al., Antigen-Down PEC Immunosensor for CYFRA21-1 Detection Based on Photocurrent Polarity Switching Strategy, 12368-73, Anal. Chem. 94 (2022), https://doi.org/10.1021/acs.analchem.2c01478.
[19] G. Zhang, X. Li, D. Chen, N. Li, Q. Xu, H. Li, et al., Internal Electric Field and Adsorption Effect Synergistically Boost Carbon Dioxide Conversion on Cadmium Sulfide@Covalent Triazine Frameworks Core–Shell Photocatalyst, Adv. Funct. Mater. (2023), https://doi.org/10.1002/adfm.202308553.
[20] Q. He, Q. Jin, C. Chen, J. Wang, S. Yuan, S. Le, et al., Ternary dual S-scheme In_2O_3/$SnIn_4S_8$/CdS heterojunctions for boosted light-to-hydrogen conversion, 416-25, J. Colloid Interface Sci. 650 (2023), https://doi.org/10.1016/j.jcis.2023.06.211.
[21] R. Shen, D. Ren, Y. Ding, Y. Guan, Y.H. Ng, P. Zhang, et al., Nanostructured CdS for efficient photocatalytic H_2 evolution: A review, Science China, Materials 63 (2020) 2153–2188, https://doi.org/10.1007/s40843-020-1456-x.
[22] J. Low, J. Yu, M. Jaroniec, S. Wageh, A.A. Al-Ghamdi, Heterojunction Photocatalysts, Adv. Mater. 29 (2017), https://doi.org/10.1002/adma.201601694.
[23] N. Song, Y. Yu, Y. Zhang, Z. Wang, Z. Guo, J. Zhang, et al., Bioinspired hierarchical self-assembled nanozyme for efficient antibacterial treatment, Adv. Mater. (2023), https://doi.org/10.1002/adma.202210455.
[24] X. Wang, Y. Fang, B. Shi, F. Huang, F. Rong, R. Que, Three-dimensional $NiCo_2O_4$@$NiCo_2O_4$ core–shell nanocones arrays for high-performance supercapacitors, Chem. Eng. J. 344 (2018) 311–319, https://doi.org/10.1016/j.cej.2018.03.061.
[25] Y. Gong, Z. Yang, Y. Lin, J. Wang, H. Pan, Z. Xu, Hierarchical heterostructure $NiCo_2O_4$@$CoMoO_4$/NF as an efficient bifunctional electrocatalyst for overall water splitting, J. Mater. Chem. A 6 (2018) 16950–16958, https://doi.org/10.1039/c8ta04325f.
[26] X. Tian, Y. Cheng, Y. Zhou, B. Zhang, G. Wang, Long-cycling and high-loading lithium-sulfur battery enabled by free-standing three-dimensional porous $NiCo_2O_4$ nanosheets, Appl. Energy 334 (2023) 120694, https://doi.org/10.1016/j.apenergy.2023.120694.
[27] C.-Q. Zhao, S.-N. Ding, Perspective on signal amplification strategies and sensing protocols in photoelectrochemical immunoassay, Coord. Chem. Rev. 391 (2019) 1–14, https://doi.org/10.1016/j.ccr.2019.03.018.
[28] W. He, L. Liu, T. Ma, H. Han, J. Zhu, Y. Liu, et al., Controllable morphology $CoFe_2O_4$/g-C_3N_4 p-n heterojunction photocatalysts with built-in electric field enhance photocatalytic performance, Appl. Catal. B: Environ. 306 (2022) 121107, https://doi.org/10.1016/j.apcatb.2022.121107.
[29] Z. Qi, J. Chen, Q. Li, N. Wang, S.A.C. Carabineiro, K. Lv, Increasing the Photocatalytic Hydrogen Generation Activity of CdS Nanorods by Introducing Interfacial and Polarization Electric Fields, Small (2023), https://doi.org/10.1002/smll.202303318.
[30] Y. Zhang, T. Wu, Q. Cui, Z. Qu, Y. Zhang, H. Ma, et al., ReS_2@Au NPs as signal labels quenching steady photocurrent generated by $NiCo_2O_4/CdIn_2S_4/In_2S_3$ heterojunction for sensitive detection of CYFRA 21-1, Biosens. Bioelectron. 222 (2023) 114992, https://doi.org/10.1016/j.bios.2022.114992.
[31] R. Yang, C. Yuan, W. Dong, Y. Ren, Y. Xue, H. Cui, Au Nanoparticle-Decorated Magnetic $CoFe_2O_4$ Core Nanoparticles Functionalized with N-(4-Aminobutyl)-N-ethylisoluminol for Detection of Copeptin, ACS Appl. Nano Mater. 5 (2022) 5925–5933, https://doi.org/10.1021/acsanm.2c01317.
[32] J. Luo, J. Luo, L. Deng, M. Yang, X. Chen, A "signal-on" photoelectrochemical sensor for human epidermal growth factor receptor 2 detection based on Y6/CdS organic–inorganic heterojunction, Microchim. Acta 189 (2022), https://doi.org/10.1007/s00604-022-05489-x.
[33] X. Ren, N. Song, J. Chen, M. Gao, H. Wang, Z.F. Gao, et al., Oxygen vacancies-driven signal enhanced photoelectrochemical sensor for mercury ions detection, Talanta 272 (2024) 125780, https://doi.org/10.1016/j.talanta.2024.125780.
[34] X. Ren, J. Chen, C. Wang, D. Wu, H. Ma, Q. Wei, et al., Photoelectrochemical Sensor with a Z-Scheme Fe_2O_3/CdS Heterostructure for Sensitive Detection of Mercury Ions, Anal. Chem. 95 (2023) 16943–16949, https://doi.org/10.1021/acs.analchem.3c03088.
[35] F.-Y. Liu, T.-K. Zhang, Y.-L. Zhao, H.-X. Ning, F.-S. Li, Electrochemiluminescence of 1,8-Naphthalimide-Modified Carbon Nitride for Cu^{2+} Detection, J. Anal. Test. 6 (2021) 296–307, https://doi.org/10.1007/s41664-021-00203-x.
[36] L. Shen, X. Jin, Z. Zhang, Y. Yi, J. Zhang, Z. Li, Extraction of Eugenol from Essential Oils by In Situ Formation of Deep Eutectic Solvents: A Green Recyclable Process, J. Anal. Test. 8 (2023) 63–73, https://doi.org/10.1007/s41664-023-00267-x.

Na Song is a master student in school of chemistry and chemical engineering, University of Jinan. His current research interests are photoelectrochemical sensor and nanomaterials.

Jingui Chen is a master student in school of chemistry and chemical engineering, University of Jinan. His current research interests are photoelectrochemical sensor and nanomaterials.

Xiang Ren received his B.S. degrees in Chemistry of Materials/English from University of Jinan in 2012, M.S. degree in Chemical Engineering and Technology from University of Jinan in 2015, and Ph.D. degree from University of Jinan/University of Electronic Science and Technology of China in 2019. Now, he is an associate professor in University of Jinan. His main research interests are energy catalysis, nanomaterials controlled-synthesis, and electrochemical biosensors.

Dan Wu is an associate professor in University of Jinan. Her main research interests are nanomaterials controlled-synthesis, and electrochemical biosensors.

Hongmin Ma is an associate professor in University of Jinan. His main research interests are energy catalysis, nanomaterials controlled-synthesis, and electrochemical biosensors.

Faying Li is an associate professor in Shandong First Medical University & Shandong Academy of Medical Sciences, His main research interests are nanomaterials controlled-synthesis, and electrochemical biosensors.

Huangxian Ju received his BS, MS and Ph.D. degrees from Nanjing University during 1982–1992. He was a postdoc in Montreal University (Canada) from 1996 to 1997 and a guest professor in three universities of Germany and Ireland in 1999–2000. He became an associate and full professor of Nanjing University in 1993 and 1999. He is currently the director of State Key Laboratory of Analytical Chemistry for Life Science. His research interests focus on analytical biochemistry, biosensing and molecular diagnosis. He has published 13 books and 785 papers in different journals with SCIE h-index of 100 (>37,500 citations) and Google Scholar h-index of 109 (> 43600 citations).

Qin Wei, a professor and DSc, has devoted herself to analytical teaching and scientific research. Her main research interests are the determination of protein and nucleic acid by photometry and the electrochemical immunosensor preparation. She has published over one hundred articles on analysis, immunosensor and applied successfully for many research projects, such as Biomaterials, Adv. Funct. Mater., Biosens. Bioelectron., Sens. Actuators B: Chem., Talanta.